# Improving the Accuracy of the Uniaxial Bias Extension Test on Engineering Fabrics Using a Simple Wrinkle Mitigation Technique

Philip Harrison*, Euan Taylor and Jafar Alsayednoor

School of Engineering, University of Glasgow, University Avenue, Glasgow, G12 8QQ, UK

## Abstract

In response to a previous investigation on the influence of specimen pre-shear and wrinkling on the accuracy of uniaxial bias extension test results [1], numerical and experimental investigations have been conducted, aimed at evaluating the use of transparent anti-wrinkle plates to mitigate errors due to wrinkling of engineering fabrics. Predictions of the numerical investigation suggest that the anti-wrinkle plates significantly improve the accuracy of kinematic measurements while introducing only a very minor stiffening effect on the axial force versus shear angle data. Results from subsequent experiments on two different engineering fabrics confirmed the numerical predictions; the accuracy and repeatability of test data was significantly improved and the maximum shear angle and axial force data measurable in the tests was significantly increased. The investigation suggests a useful role for anti-wrinkle plates in characterising the formability of engineering fabrics.

Key words:

## 1. Introduction

The Uniaxial Bias Extension test (UBE) [2–6] is a commonly used technique to characterise the shear stiffness of engineering fabrics and composite prepregs. Normalisation methods can be employed to extract the underlying shear stiffness for both rate independent fabrics [7–11] and rate dependent prepregs (assuming Newtonian rate dependence) [12]. Though, due to the very different adhesive and frictional properties of dry fabrics and prepregs, the techniques applied in this investigation are currently applicable only to dry fabrics. A recent modification to the test [13,14], designed to create a rigid material behaviour in Region C of the test specimen in engineering fabrics, mitigates intra-ply slip, creates an encastre-style boundary condition at the interface between Regions B and C (see Figure 1) and consequently enables information on both the in-plane bending stiffness (a 2$^{nd}$ order gradient effect) [13,15–20] and the torsional stiffness of a fabric subject to large shear deformations [13] to be determined via inverse modelling. The UBE test has even been employed to investigate the integrity and cohesion of engineering fabrics [21,22].

Ultimately these measurements, combined with results from complementary tensile, bending and compaction tests, can be used to determine the parameters of constitutive models designed for use in mechanical forming simulations of fabric sheets, with the aim of predicting information such as fibre

direction (for use in liquid moulding simulations or structural simulations [23,24]) and defects such as out-of-plane wrinkling [25,26] or in-plane fibre kinking [27]. Forming simulations can be used to predict the effect of changing boundary conditions on the deformation of the forming fabric blank [28] and can ultimately be employed to optimise manufacture conditions [29] with the goal of producing defect free advanced composite components with fibres optimally oriented to support anticipated in-service loads.

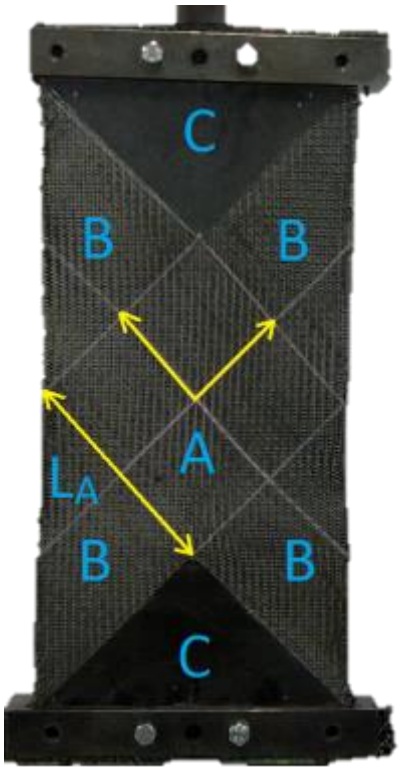


*Figure 1. Uniaxial bias extension test specimen: Three regions can be identified in the specimen A-C. Aluminium is bonded using epoxy adhesive in Region C (here the aluminium foil has been painted black to reduce reflections). The side length of Region A, $L_A$, is used to analyse the test results.*

Precise mechanical characterisation is a necessary precondition for accurate simulations. Nevertheless, comparison of results measured using the UBE test made by different research groups on the same fabrics demonstrated a large amount of variation both within datasets from the same group and also between the datasets of the different research groups [9]. A recent investigation [1] highlighted that much of the variability is caused, not by inherent material variations but by imperfect sample preparation, the method used to analyse results and by specimen wrinkling. ***Specimen pre-shear*** prior to starting the UBE test is one notable source of error. For example, close examination of Figure 1 reveals a pre-shear error of about 1° (detectable here by comparing the white lines marked on the tow directions of the fabric specimen with the superimposed perfectly orthogonal yellow arrows). A first step to improve the quality of UBE test results is to eliminate specimen pre-shear as much as possible. Reporting the average pre-shear angle and the standard deviation of the pre-shear angle obtained from a given dataset can improve confidence in the results. For example, an average pre-shear angle of less than ~0.5° and a standard deviation of the initial pre-shear angle less than ~2° has been empirically shown to produce highly repeatable data [1]. In addition, the adverse influence of any unintended pre-shear can be mitigated when analysing results by simple modification of standard equations for interpreting sample kinematics [1].

***Out-of-plane wrinkling*** often occurs towards the later stages of a UBE test in woven fabrics (though in some fabrics, such as certain non-crimp fabrics, experience shows that wrinkles do not occur at all due to the absence of shear locking). The wrinkle onset angle and subsequent development of wrinkles in a UBE test depend on the fabric's mechanical forming properties and the size of the test specimen; larger specimens tend to begin wrinkling at lower shear angles and the wrinkle amplitude tends to be more severe [13] (note that in-plane fabric tension is also known to influence the development of wrinkles [30,31], but given that in a UBE test, the fabric tension is itself a function of both the material's mechanical properties and specimen size, its involvement in wrinkle generation during the UBE test is implicitly assumed and effectively modelled if the axial force can be accurately predicted when simulating the test). The dependence of the wrinkle onset angle on the fabric's mechanical properties mean that measuring it can help in identifying certain properties; in particular, the torsional stiffness of the sheared fabric [13]. This makes wrinkle onset angle measurements valuable information in the material characterisation process. Nevertheless, out-of-plane fabric wrinkling is a significant source of error when measuring shear angle data during the later stages of the UBE test. Any non-orthogonality of the specimen surface in relation to the observer changes the perceived shear angle measured from the surface of the specimen. Wrinkling creates a complex undulating surface, usually at the centre of the test specimen [13,1,32–34] precisely where shear angle kinematics tend to be measured (see Figure 1). The amount by which the perceived shear angle is influenced by the wrinkle depends on its exact form. To complicate matters, the same type of woven fabric tested in the UBE test can produce wrinkles of differing shape, implying that wrinkle development is sensitive to small perturbations in sample preparation. In Alsayednoor et al. 2017 [1], the effect of a wrinkle measured using 2-D recording techniques (as opposed to stereographic full-field digital image correlation) was to significantly increase the perceived shear angle at the centre of the specimen by as much as 20%. In the current investigation we explore the viability of a technique, involving the use of transparent anti-wrinkle plates to constrain and thereby mitigate the growth of wrinkles.

The remainder of this paper is structured as follows. In Section 2, a brief numerical investigation is presented to examine the influence of adding transparent anti-wrinkle plates to the standard UBE test, on both the development of wrinkles and also on the observed kinematics and force versus shear angle data. Results of the numerical investigation provide the motivation behind the experimental investigation reported in Section 3. The latter begins with a description of two fabrics employed in the investigation before detailing the experimental setup and finally a discussion of the results. Conclusions of the investigation are provided in Section 4.

## 2. Numerical Investigation into Influence of Rigid Anti-Wrinkle Plates

Numerical simulations were run to examine the effect of adding front and back rigid anti-wrinkle plates to the standard UBE test (see Figure 2B). The approach used the mutually constrained pantographic beam and membrane finite element model [13,14] implemented in Abaqus Explicit™. The models were assigned the material properties of the (untreated) carbon fabric characterised previously in [13] (see Section 3.1) and had a height of 416.3mm and a width of 203.7mm giving an aspect ratio of 2.04. This specific simulation was chosen as it was known to develop a wrinkle after about 38° of shear. Two further variations of the simulation were run such that:

- Simulation 1: No constraining anti-wrinkle plates
- Simulation 2: Constraining anti-wrinkle plates at the front and back of the sample with a gap of 0.5mm between them and a coefficient of friction of 0 between the specimen and the plates

- Simulation 3: The same as Simulation 2 but with a coefficient of 0.3 between the specimen and the plates

A penalty contact condition was applied between the surface of the membrane elements and the rigid body anti-wrinkle plates. Figure 2 shows the results of the three simulations. The plates clearly inhibit the development of the wrinkle in the test specimen. The question is whether this constraint on out-of-plane motion (in the Z-direction) adversely affects: (i) the kinematics and (ii) the axial force measured during the test; Sections 2.1 and 2.2 examine this question.

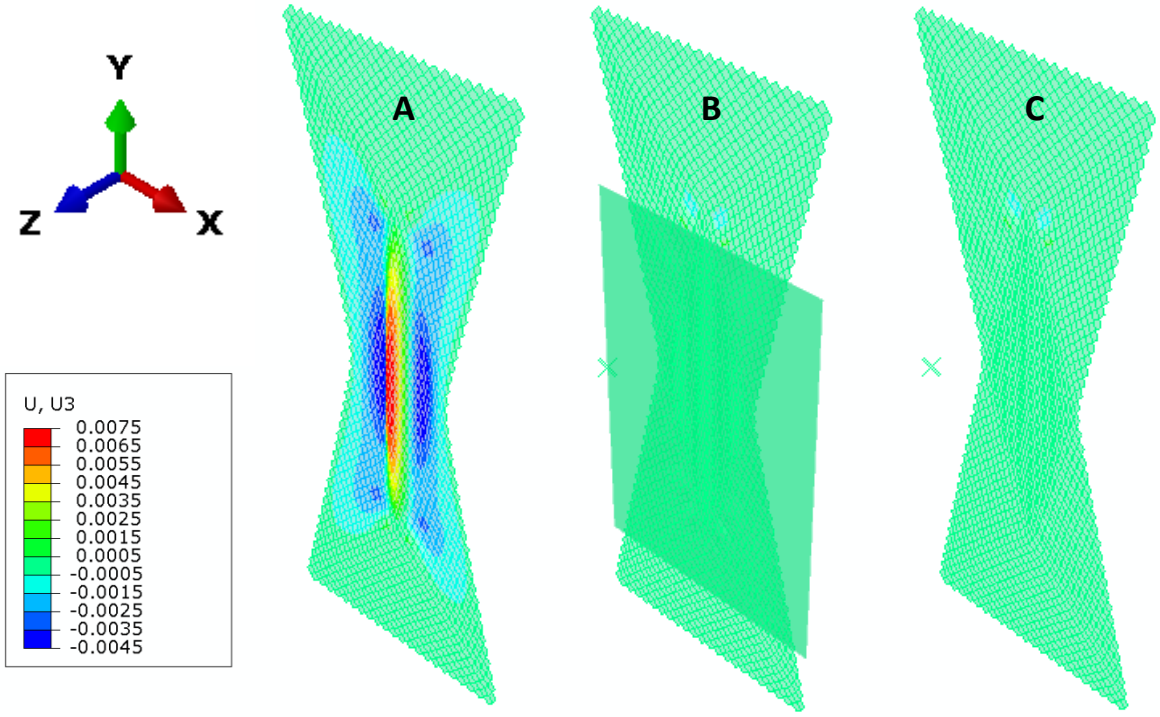


*Figure 2. The colour legend indicates out-of-plane displacement (in metres) and applies to all three simulations. (A) Simulation 1 (without constraining plates) develops an obvious out-of-plane wrinkle, (B) Simulation 2 shows that the two frictionless plates (translucent in this image) mitigate the development of the wrinkle, (C) Simulation 3 also includes plates (with friction), but these are removed in this image to more clearly see the specimen.*

## 2.1 Influence of Anti-Wrinkle Plates on Measured Shear Kinematics

A MatLab script was used to convert the Abaqus output files into a series of images in which the fibre directions are clearly visible and suitable for manual image analysis (see, for example, Figure 3C in [1]). Every 10$^{th}$ frame (from a total of 400) was manually analysed to manually measure the shear angle at the centre of Region A (see Figure 1) when viewed from a perfectly orthogonal perspective relative to the plane of the specimen. These measured shear angle values were then plotted against the theoretical shear angle predicted for ideal trellis shear kinematics (calculated using the Y-displacement of the top of the specimen). The results are shown in Figure 3 for each of the three simulations (plotted as data points), also plotted is the true shear angle predicted in Simulation 1 (shown as a red line in Figure 3). Note that, at low to moderate shear angles, the true shear angle lies above the theoretical angle predicted by ideal shear kinematics (the black line). This is a consequence of adding an in-plane bending stiffness in the simulation and is an observation that has previously been verified experimentally [13]. At high shear angles (>70$^{o}$), the true shear angle predicted in Simulation 1 begins to drop below the ideal shear angle (the black line) due to extension along the fibre directions. The

results show that the measured shear angle in the two simulations incorporating rigid plates (Simulations 2 & 3) lay very close to the true shear angle predicted in Simulation 1. The presence of friction between the specimen and the plates has very little influence; Simulations 2 and 3 give almost the same result. In contrast, after the wrinkle begins to form, the measured shear angle in Simulation 1 significantly diverges from the true predicted shear angle (overestimating the true shear angle by as much as 20%, as in [1]). The results suggest that *using anti-wrinkle plates has little effect on the shear angle versus axial displacement behaviour of the specimen but does significantly improve the accuracy of manual 2D kinematic measurements.*

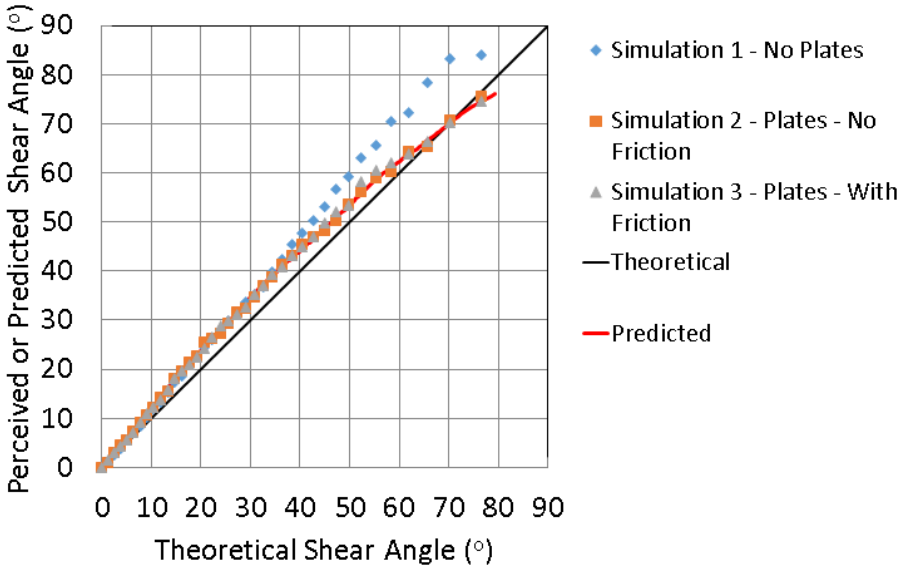


*Figure 3. The data points show the measured shear angle manually measured from Simulations 1 to 3 as well as the true shear angle predicted by Simulation 1.*

## 2.2 Influence of Anti-Wrinkle Plates on Axial Force Predictions

The axial force output from Simulations 1 to 3, normalised by the side length of Region A (see Figure 1) is plotted against the predicted shear angle at the centre of Region A for each specimen in Figure 4.

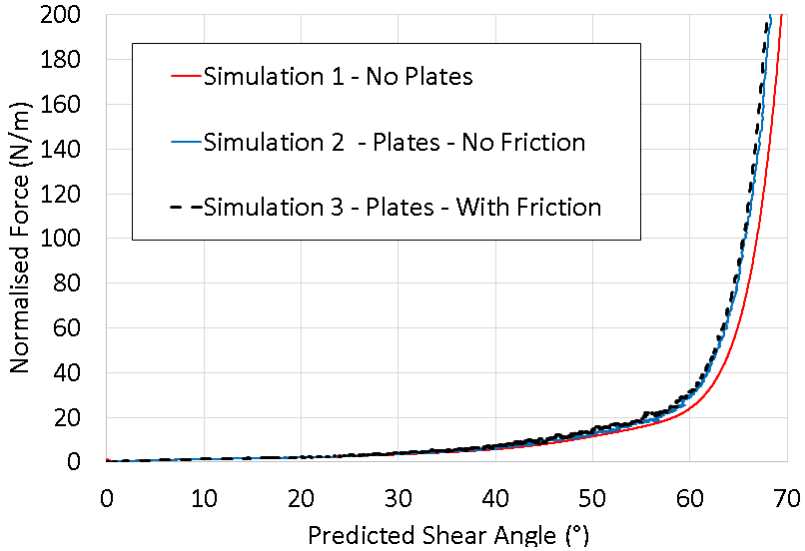


*Figure 4. Normalised axial force predictions versus the predicted shear angle at the centre of Region A for Simulations 1 to 3.*

As might be expected, the results show that adding the constraint on out-of-plane motion slightly stiffens the apparent measured response (Simulations 2 and 3) compared to the unconstrained specimen (Simulation 1), i.e. at a given force the shear angle is decreased by, at most, ~3%. Adding friction between the specimen and the plates appears to have a very minor influence on the force response (compare Simulation 2 with Simulation 3). Figure 5 shows the normal force exerted by the wrinkle on the anti-wrinkle plate versus the specimen shear angle. The predicted reaction force is very low at shear angles less than 60° then rapidly grows. Based on this result, simple calculations using Coulomb's Law suggest the friction could contribute around 4% of the measured axial force at ~60° of shear and more than 10% at ~65°, though these relatively large contributions are not seen in the axial force predictions of Figure 4 (a point that currently remains an unsolved puzzle). Further discussion of this prediction is provided in Section 3.2.

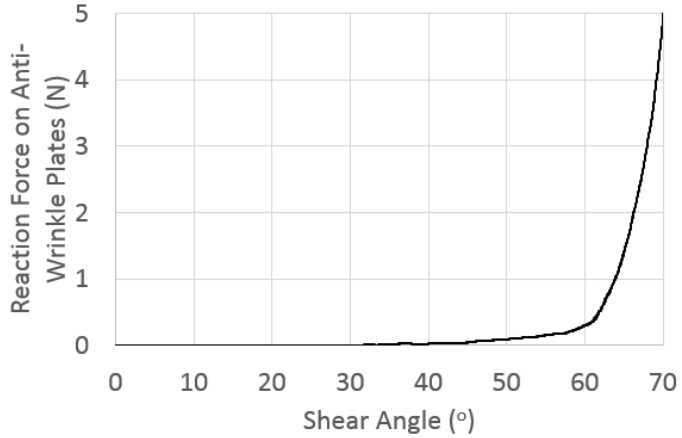


*Figure 5. Prediction of wrinkle reaction force against anti-wrinkle plates versus shear angle at centre of Region A of the UBE specimen.*

The numerical predictions suggest that *the apparent increase in specimen stiffness caused by introducing the plates is much lower than the apparent decrease in specimen stiffness attributable to the erroneously high shear angle measurements associated with specimen wrinkling* (see Section 2.1 and [1]). In other words, the numerical investigation suggests that the improvement in accuracy related to more precise kinematic measurements (eliminating errors in the shear angle of up to 20%) outweighs the reduction in accuracy due to the increase in apparent stiffness of the specimen (introducing errors in the shear angle of up to 3%). This encouraging result provides the motivation behind the subsequent experimental investigation.

# 3. Experimental Investigation

Two engineering fabrics have been tested both with and without anti-wrinkle plates. Kinematic and force measurements are compared to evaluate the influence of the plates on the resulting data.

## 3.1 Materials

Fabric 1 (see Figure 6A) is a 2x2 twill weave engineering carbon fabric (from EasyComposites) with an areal density of 0.21± 0.002$kg/m^2$ and an average thickness of 0.2+/-0.021m (the same fabric was used in [13]. Fabric 2 (see Figure 6B) is a plain weave glass fabric (from Allscot - code ECK 10) with an areal density of 0.30 ± 0.01$kg/m^2$ and an average thickness of 0.26+/-0.02mm. Figure 6 shows that the glass fabric has a more open structure than the carbon fabric.

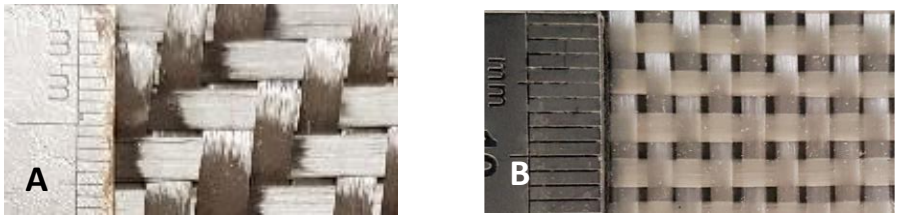


*Figure 6. Close up image of fabric weaves. (A) carbon twill weave (B) glass plain weave. A scale rule indicates the dimensions of the fabric meso-structures.*

## 3.2 Experimental Setup

All samples were tested using a Zwick Z2 tensile test machine fitted with a 2KN load cell using a displacement rate of 200mm/min. Specimen dimensions were 200x400mm. Aluminium was bonded on Region C (see Figure 6B). Tests were filmed from the front using a Casio HS EXZR-700 digital camera (to record the shear angle – see Figure 1 and 7B) and from the rear using a Samsung Galaxy S8 smartphone (to record wrinkle development – see Figures 7C, 8 and 9). The videos were divided into still frames using Virtual Dub software, 2 frames per second were retained for analysis. ImageJ software [35] was used to manually measure the shear angle at the centre of Region A using lines marked along the tows. Shear angle measurements were repeated 3 times for each test and each test was repeated 4 times. The average shear angle for each image was determined and the standard deviation was used to plot the error bars on each data point (see Figures 10 and 11), providing an indication of the human error involved in performing the measurements. Perspex anti-wrinkle plates were manufactured with a 2mm gap between front and back plates. The plates were hinged on one side with a 2mm spacer plate on the other. Specimens were loaded in the test machine (see Figure 7B), and the plates were positioned and held in place using G-clamps (see Figure 7A). Initial attempts to use small magnets to lock the anti-wrinkle plates in position were abandoned as the wrinkle would push the plates open, indicating a wrinkle reaction force of several Newtons (as also indicated in Figure 5). This simple experimental observation together with the wrinkle reaction force prediction shown in Figure 5 suggests another possible evaluation of forming models – namely, comparison of the measured and predicted wrinkle reaction forces, using instrumented anti-wrinkle plates, an endeavour deferred to future investigations. Two sets of tests were conducted on each type of fabric, one without the anti-wrinkle plates the other with the plates.

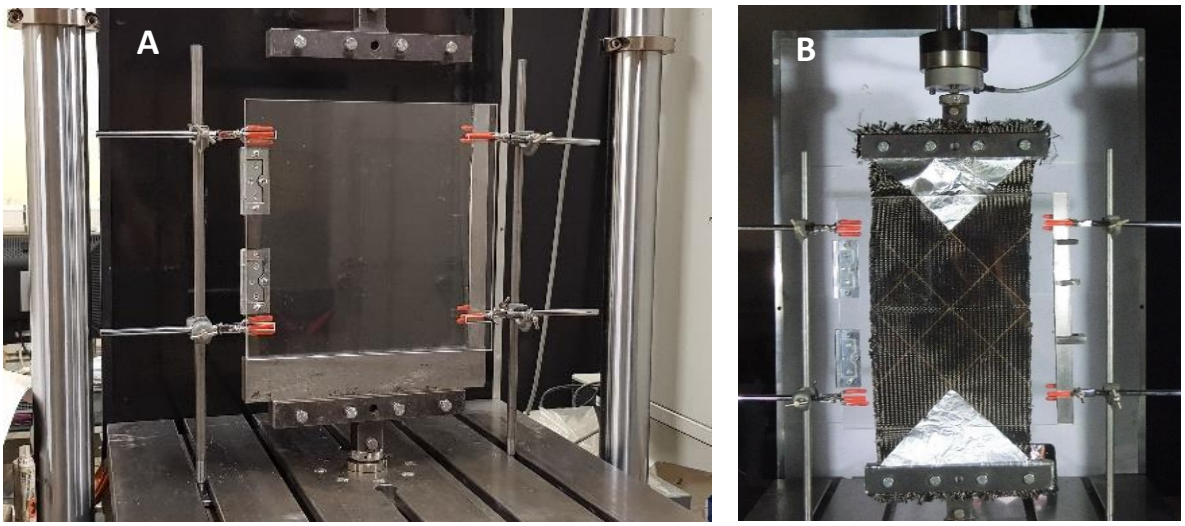

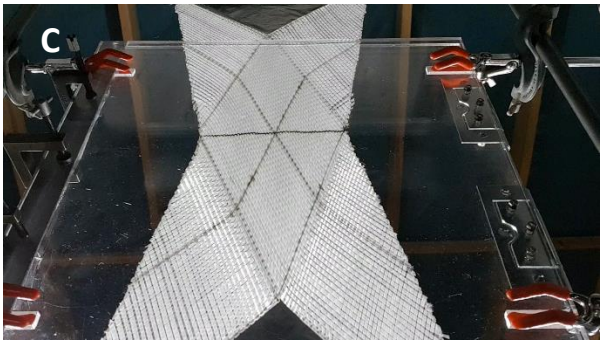


*Figure 7. (A) Perspex anti-wrinkle plates and clamps. (B) front view of carbon UBE test specimen positioned between the anti-wrinkle plates prior to testing (C) back view of glass UBE specimen positioned between the anti-wrinkle plates during testing*

## 3.3 Wrinkle Onset Angle

As discussed in Section 1, the wrinkle onset angle can be useful in determining the torsional stiffness of the sheared fabric via inverse modelling [13]. Using an oblique viewing perspective (see Figure 8), the wrinkle onset angle was measured from UBE tests conducted without the anti-wrinkle plates. The gradual onset and evolution of the wrinkles makes this a rather subjective measurement, nevertheless, values were estimated from the recorded videos and given in Table 1. Results indicate that the glass fabric tends to wrinkle earlier than the carbon fabric, suggesting that despite the more open meso-structure (see Figure 6) the plain weave glass fabric is less formable than the carbon fabric. Note that a definitive criterion for deciding when a slight buckle becomes a 'wrinkle' has yet to be established, partly explaining why the wrinkle onset angle measured here for the carbon fabric (~49°) is considerably larger than the wrinkle onset angle measured for the same fabric in [13], i.e. ~40°.Though this can perhaps also be explained by the fact that different optical techniques were used to measure the wrinkle onset angle in the two investigations; the current oblique viewing method is likely to be more accurate than analysis of orthogonal perspective videos (and is also much closer to the wrinkle onset angle of 50° measured using DIC in [13]).

*Table 1. Wrinkle onset angle measured in the UBE tests for the carbon and glass fabrics.*

| | Wrinkle Onset Angle (°) | | | | | |
|---|---|---|---|---|---|---|
| **Sample No.** | **1** | **2** | **3** | **4** | **Average** | **SD** |
| **Carbon No Plates** | 46.3 | 50.7 | 47.6 | 52.3 | 49.2 | 2.8 |
| **Glass No Plates** | 49.9 | 47.0 | 44.9 | 43.9 | 46.4 | 2.7 |

As expected, when using the anti-wrinkle plates the specimens are prevented from wrinkling. Figure 9 shows the glass fabric specimens at a vertical displacement of 64mm, viewed from an oblique perspective. The form of the specimens can be directly compared with Figure 8 (without plates). The planarity of the specimens is obviously much improved, facilitating more accurate shear angle measurements. Similar results were also found with the carbon fabric (not shown here).

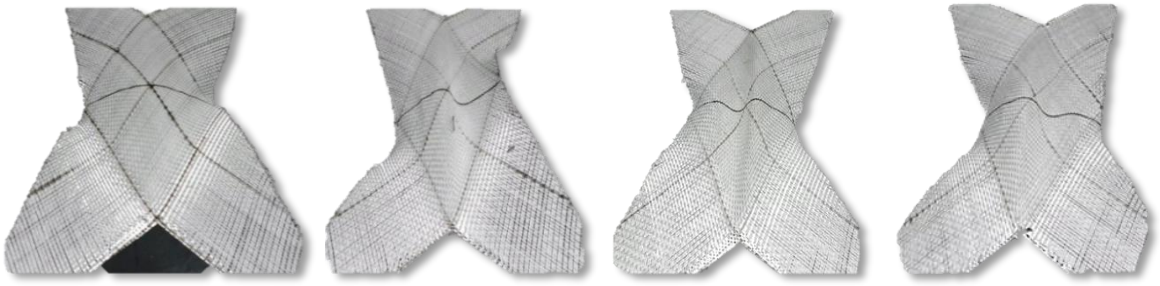

*Figure 8. Unconstrained UBE glass fabric specimens at a displacement of 64mm during the tests. The specimens are viewed from below such that the initially straight horizontal line, marked across the mid-height of the test specimen can be used to observe the morphology of the developing wrinkle throughout the course of the test*

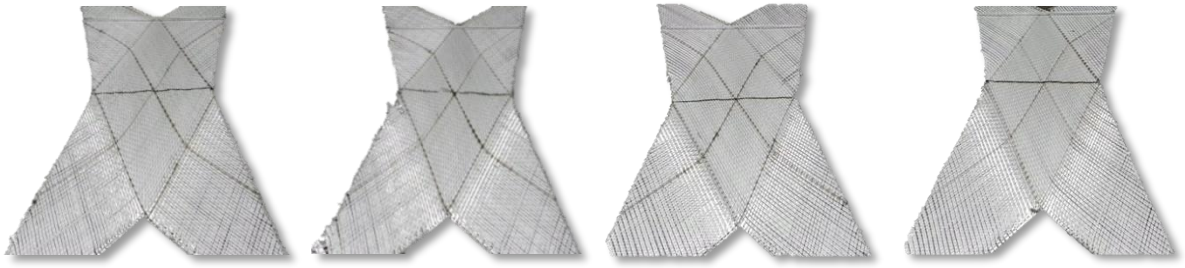

*Figure 9. Effect of Perspex anti-wrinkle plates on planarity of the four UBE glass fabric specimens at a displacement of 64mm during the tests.*

## 3.4 Influence of Anti-Wrinkle Plates on Experimentally Measured Shear Kinematics

The measured shear angle was plotted against the theoretical shear angle for the carbon and glass fabrics, tested both with and without the anti-wrinkle plates. Equation (1) was used to calculate the theoretical shear angle

$$\theta = \frac{\pi}{2} - 2acos\left[\frac{d}{2L_A(\lambda-1)} + cos\frac{\emptyset_{initial}}{2}\right] \quad (1)$$

where $L_A$ is the side length of Region A (see Figure 1), *d* is the vertical displacement of the top of the test specimen, $\lambda$ is the aspect ratio of the test specimen ($\lambda$ =2 in these experiments), $\emptyset_{initial}$ is the initial inter-fibre angle at the start of the test and $\theta$ is the shear angle at the centre of Region A [13,1]. As discussed in Section 1, the average pre-shear angle and its standard deviation are a good indicator of the care taken in preparing and installing the tests specimens [1]. This information is provided for the four datasets in Table 2.

*Table 2: Average pre-shear angle and standard deviation of the pre-shear angle for each of the four datasets*

| | Test Method | Average Pre-shear Angle (°) | Std. Dev (°) |
|---|---|---|---|
| **Carbon** | No Screen | -0.30 | 0.10 |
| | Screen | -0.16 | 0.67 |
| **Glass** | No Screen | 0.41 | 1.08 |
| | Screen | -0.15 | 0.39 |

Kinematic results from the four datasets are shown in Figure 10. As discussed in Section 1, such data is useful in determining the in-plane bending stiffness of the fabrics [13,14] and also indicates the shear angle at which intra-ply becomes significant; the shear angle at which the measured angle drops below the theoretical angle. However, to be useful the data must be accurately measured. Figure 10 shows that the variability of results measured without the anti-wrinkle plates is clearly much larger than when measured with the anti-wrinkle plates for both types of fabric. Figures 10A and 10C show that above the wrinkle onset angle, some of the data lie well above the theoretical prediction; an effect predicted in the numerical investigation and attributable to the wrinkle on the perceived angle measurement – see Section 2.1. The significantly improved repeatability of data in Figures 10B and 10D, provides strong justification for use of the anti-wrinkle plates when measuring shear angle kinematics in a UBE test.

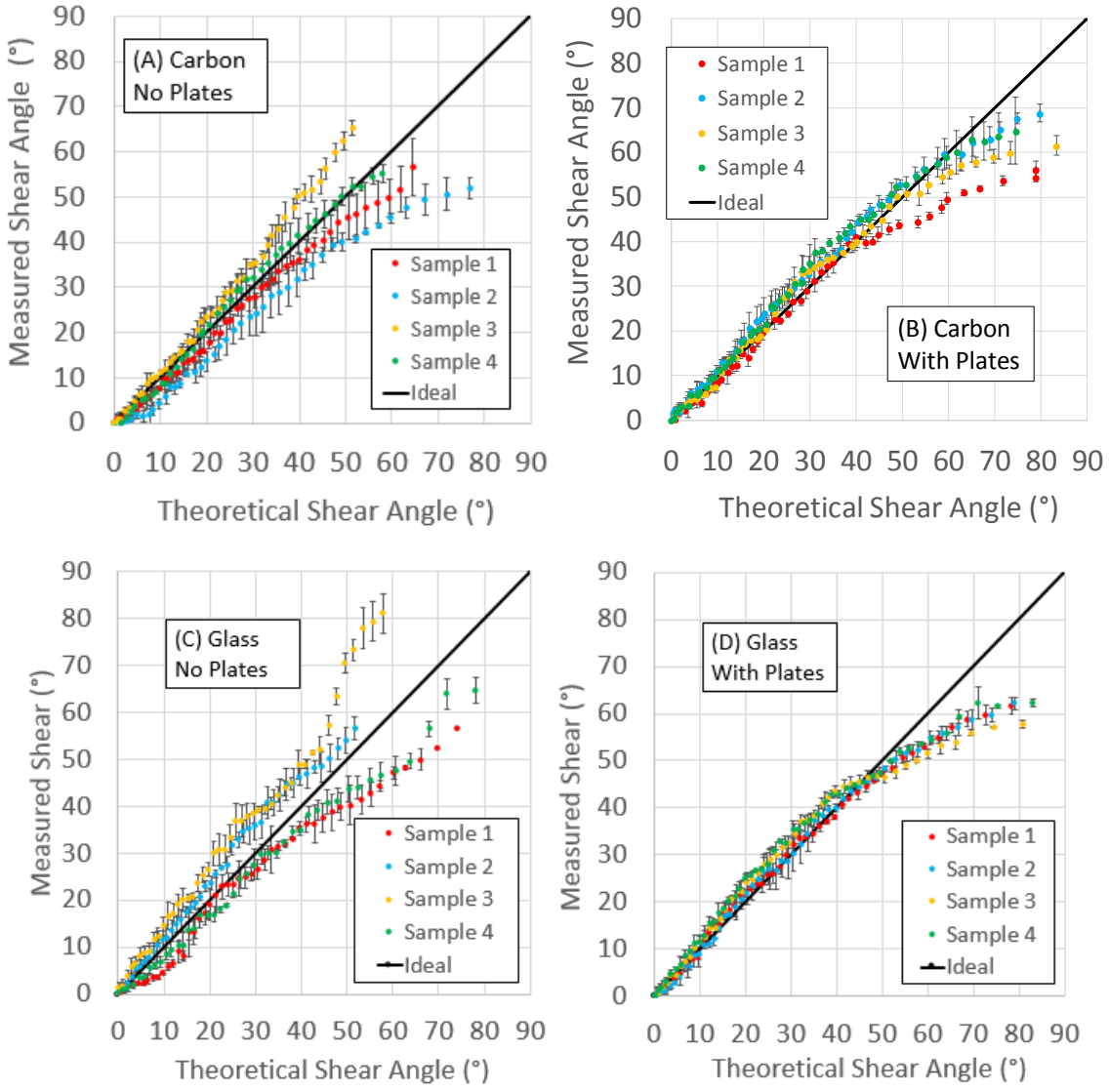


*Figure 10. Measured versus theoretical shear angle for: (A) Carbon fabric without anti-wrinkle plates (B) Carbon fabric with anti-wrinkle plates (C) Glass fabric without anti-wrinkle plates (D) Glass fabric with anti-wrinkle plates*

## 3.5 Influence of Anti-Wrinkle Plates on Experimentally Measured Axial Force

The axial force is normalised using the side length of Region A of the test specimen, $L_A$. The occurrence of wrinkling in the unconstrained UBE tests made measurement of the shear angle difficult. For this reason, only a limited amount of data could be collected at high shear angles (see Figures 11A and 11C). In contrast, the lack of wrinkling when using the anti-wrinkle plates allowed reliable shear angle versus axial force measurements to be made at much higher shear angles (see Figures 11B and 11D).

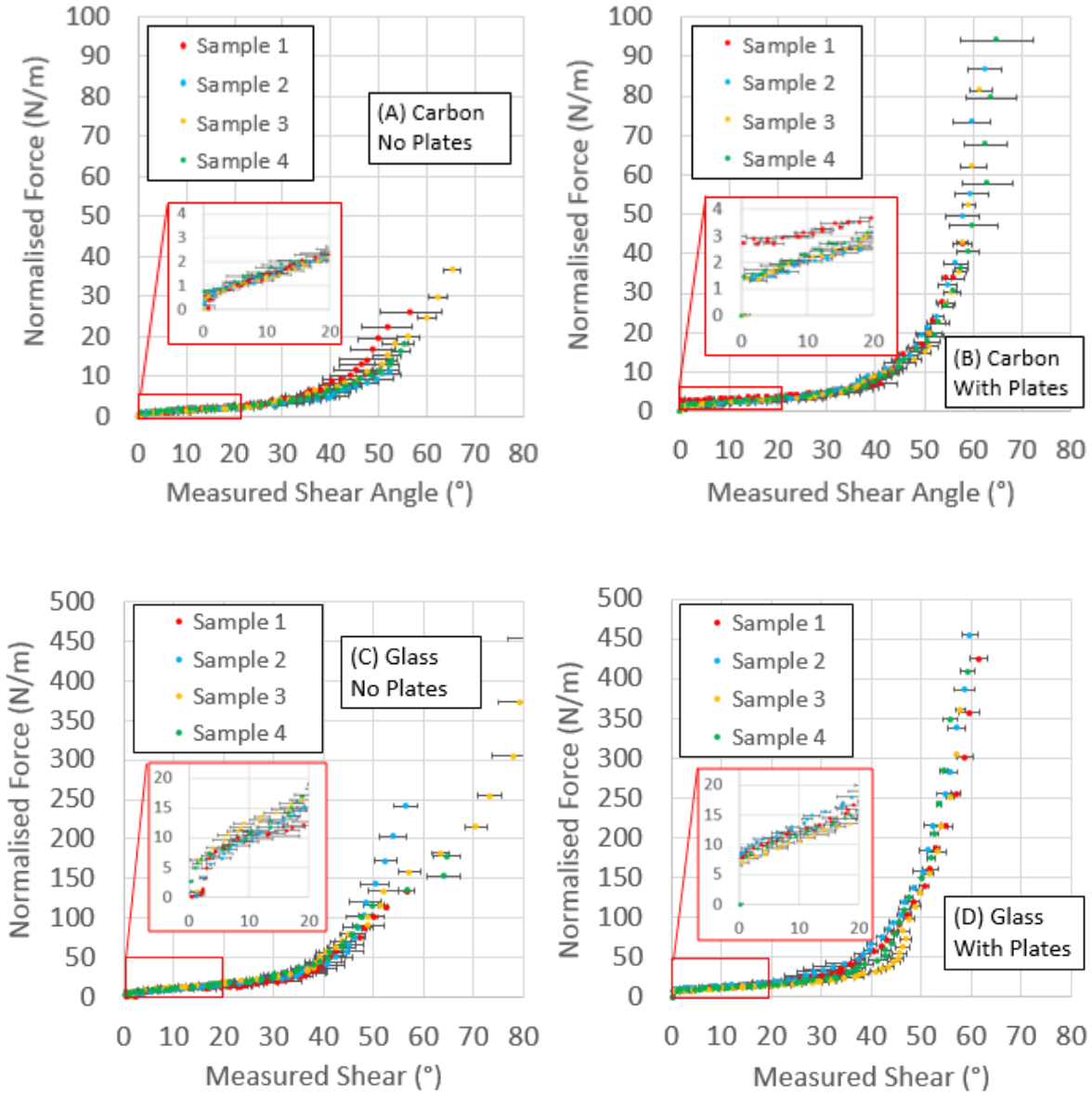


*Figure 11. Normalised axial force versus measured shear angle for: (A) Carbon fabric without anti-wrinkle plates (B) Carbon fabric with anti-wrinkle plates (C) Glass fabric without anti-wrinkle plates (D) Glass fabric with anti-wrinkle plates.*

Once again use of anti-wrinkle plates provided more reliable data, especially at high shear angles. However, unlike the numerical investigation, the influence of friction between the specimen and the anti-wrinkle plates is evident at very low shear angles, probably due to imperfect alignment between the specimen and the plates. Figures 11B and 11D both show a small increase in the axial force at low shear angles due to friction (compared with Figures 11A and 11C). To demonstrate this issue, zoomed

insets in Figure 11 show close-up images of the data at low shear angles. Given the very low shear force in the fabrics at these low shear angles, the resulting signal to noise ratio is high. A solution is to combine the pre-wrinkling onset shear angle data from experiments conducted without anti-wrinkle plates with the post-wrinkling onset shear angle data from experiments conducted with the anti-wrinkle plates. Specifically, data from the tests without the anti-wrinkle plates, obtained at shear angles lower than ~30$^{o}$ was simply combined with data from the tests with the anti-wrinkle plates from shear angles greater than ~30$^{o}$. This combined data is plotted in Figure 12 (blue data points). 6$^{th}$ order polynomial trend lines have been fitted to the data for both fabrics (red lines).

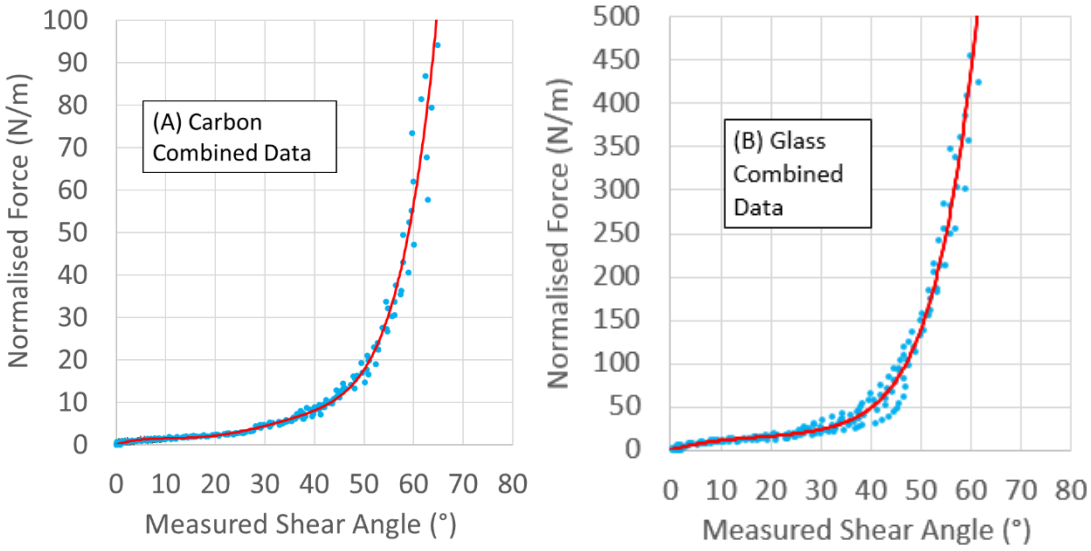


*Figure 12. Combined normalised axial force versus measured shear angle data for: (A) the carbon fabric and (B) the glass fabric.*

As a final illustration of the benefits of using the anti-wrinkle plates, in Figure 13 data presented previously in [13], measured on the same type of carbon fabric as that characterised in this investigation (but without anti-wrinkle plates), is plotted against the data measured in this investigation (from Figure 12A). Conclusions from the numerical investigation suggest that the true result should lay between the two curves. Data measured using the anti-wrinkle plate are expected to be slightly too stiff (shifted slightly upwards) whereas data measured in [13] without the plates are expected to be significantly too compliant at high shear angles (shifted downwards). Use of the anti-wrinkle plates allows the collection of data points up to much higher shear angles and axial forces than without the plates.

It is worth considering the possibility of extending the technique to prepregs. This would clearly be a challenge due to the adhesive, high friction interface between the prepreg and the antiwrinkle plates. However, techniques to lubricate the interface could be devised (e.g. via treatment with low viscosity transparent lubricating oil) and a switch from acrylic to borosilicate glass could facilitate high temperature testing, providing scope for further investigation.

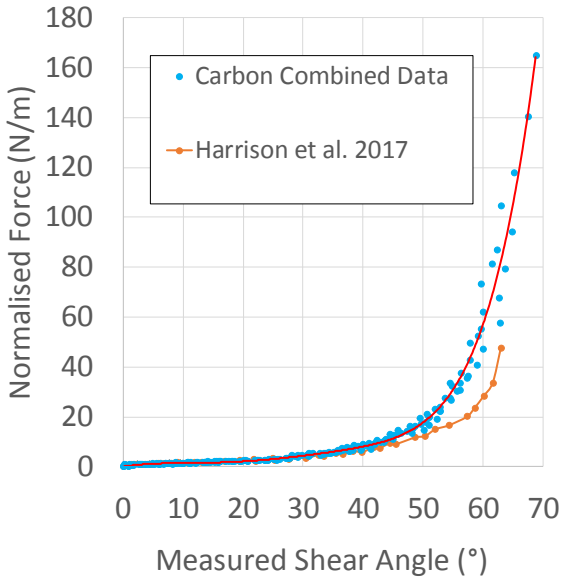


Figure 13. *Data from Figure 11A plotted together with similar data measured on the untreated 200 x 400mm carbon fabric specimen from*[13].

## 4. Conclusions

The investigation has used both numerical and experimental evidence to demonstrate the benefits of incorporating transparent anti-wrinkle plates in UBE tests on engineering fabrics; data can be measured more accurately, to higher shear angles and therefore also to higher forces. Using anti-wrinkle plates has little effect on the shear angle versus displacement behaviour of the specimen but does significantly improve the accuracy and repeatability of manual 2D kinematic measurements. The apparent increase in specimen stiffness caused by introducing the plates is much lower than the apparent decrease in specimen stiffness attributable to the erroneously high shear angle measurements associated with specimen wrinkling. Nevertheless, the need to measure the wrinkle onset angle and to record axial force versus measured shear angle data in the early stages of the test, without the influence of possible friction with the plates, means that UBE tests without anti-wrinkle plates are also very useful in the characterisation process. Consequently, in order to achieve a complete dataset with the highest quality data, it is recommended that UBE tests both with and without anti-wrinkle plates are performed.

## Acknowledgements

The authors wish to thank Engineering and Physical Sciences Research Council for the grant '2-D Forming of Low Cost Steered Fibre Laminates', (Ref: EP/P021573/1).

## References

[1] Alsayednoor J, Harrison P, Yu WR. Influence of specimen pre-shear and wrinkling on the accuracy of uniaxial bias extension test results. Compos Part A Appl Sci Manuf 2017;101:81–97. doi:10.1016/j.compositesa.2017.06.006.

[2] Cooper DNE. A Bias Extension Test. Text Res J 1963:315–7. doi:10.1177/004051755802800503.

[3] Lebrun G, Bureau MN, Denault J. Evaluation of bias-extension and picture-frame test methods for the measurement of intraply shear properties of PP/glass commingled fabrics.

Compos Struct 2003;61:341–52. doi:10.1016/S0263-8223(03)00057-6.

[4] Boisse P, Hamila N, Guzman-Maldonado E, Madeo A, Hivet G, Dell???Isola F. The bias-extension test for the analysis of in-plane shear properties of textile composite reinforcements and prepregs: a review. Int J Mater Form 2017;10:473–492. doi:10.1007/s12289-016-1294-7.

[5] Pierce RS, Falzon BG, Thompson MC, Boman R. A low-cost digital image correlation technique for characterising the shear deformation of fabrics for draping studies. Strain 2015;51:180–9. doi:10.1111/str.12131.

[6] Machado M, Fischlschweiger M, Major Z. Composites : Part A A rate-dependent non-orthogonal constitutive model for describing shear behaviour of woven reinforced thermoplastic composites 2016;80:194–203. doi:10.1016/j.compositesa.2015.10.028.

[7] Launay J, Hivet G, Duong A V., Boisse P. Experimental analysis of the influence of tensions on in plane shear behaviour of woven composite reinforcements. Compos Sci Technol 2008;68:506–15. doi:10.1016/j.compscitech.2007.06.021.

[8] Harrison P, Wiggers J, Long AC. Normalisation Of Shear Test Data for Rate-Independent Compressible Fabric. AIP Conf Proc 2007;907:1011–6. doi:10.1063/1.2729646.

[9] Cao J, Akkerman R, Boisse P, Chen J, Cheng HS, de Graaf EF, et al. Characterization of mechanical behavior of woven fabrics: Experimental methods and benchmark results. Compos Part A Appl Sci Manuf 2008;39:1037–53. doi:10.1016/j.compositesa.2008.02.016.

[10] Harrison P, Hartel F. Erratum: “Evaluation of normalisation methods for uniaxial bias extension tests on engineering fabrics” (Composites: Part A (2016) 80 (104-106)). Compos Part A Appl Sci Manuf 2016;80:104–6. doi:10.1016/j.compositesa.2015.10.013.

[11] Harrison P, Wiggers J, Long AC. Normalization of Shear Test Data for Rate-independent Compressible Fabrics. J Compos Mater 2008:1–30. doi:10.1177/0021998308095367.

[12] Harrison P, Clifford MJ, Long AC. Shear characterisation of viscous woven textile composites: A comparison between picture frame and bias extension experiments. Compos Sci Technol 2004;64:1453–65. doi:10.1016/j.compscitech.2003.10.015.

[13] Harrison P, Alvarez MF, Anderson D. Towards comprehensive characterisation and modelling of the forming and wrinkling mechanics of engineering fabrics 2017;0:1–17. doi:10.1016/j.ijsolstr.2016.11.008.

[14] Harrison P. Modelling the forming mechanics of engineering fabrics using a mutually constrained pantographic beam and membrane mesh. Compos Part A Appl Sci Manuf 2016;81:145–57. doi:10.1016/j.compositesa.2015.11.005.

[15] Cuomo M, Dell Isola F, Greco L. Simplified analysis of a generalized bias-test for fabrics with two families of inextensible fibers Simplified analysis of a generalized bias-test for fabrics with two families of inextensible fibers. Compos PART A 2016;110:177–87. doi:10.1016/j.compscitech.2016.11.003.

[16] Ferretti M, Madeo A, dell’Isola F, Boisse P. Modeling the onset of shear boundary layers in fibrous composite reinforcements by second-gradient theory. Zeitschrift Fur Angew Math Und Phys 2014;65:587–612. doi:10.1007/s00033-013-0347-8.

[17] D’Agostino M V., Giorgio I, Greco L, Madeo A, Boisse P. Continuum and discrete models for structures including (quasi-) inextensible elasticae with a view to the design and modeling of composite reinforcements. Int J Solids Struct 2015;59:1–17.

doi:10.1016/j.ijsolstr.2014.12.014.

[18] Turco E, dell'Isola F, Cazzani A, Rizzi NL. Hencky-type discrete model for pantographic structures: numerical comparison with second gradient continuum models. Zeitschrift Für Angew Math Und Phys 2016;67:85. doi:10.1007/s00033-016-0681-8.

[19] Steigmann DJ, Dell'Isola F. Mechanical response of fabric sheets to three-dimensional bending, twisting, and stretching. Acta Mech Sin Xuebao 2015;31:373–82. doi:10.1007/s10409-015-0413-x.

[20] Giorgio I. Numerical identification procedure between a micro-Cauchy model and a macro-second gradient model for planar pantographic structures. Zeitschrift Für Angew Math Und Phys 2016;67:95. doi:10.1007/s00033-016-0692-5.

[21] Harrison P, Tan MK, Long a C. Kinematics of Intra-Ply Slip in Textile Composites during Bias Extension Tests. 8th Int. ESAFORM Conf. Mater. Form., Cluj-Napoca, Romania: 2005, p. 2–5.

[22] Pan N, Kovar R, Dolatabadi MK, Wang P, Zhang D, Sun Y, et al. Origin of tensile strength of a woven sample cut in bias directions. R Soc Open Sci 2015;2:1–18. doi:10.1098/rsos.140499.

[23] Pierce RS, Falzon BG, Thompson MC. A multi-physics process model for simulating the manufacture of resin-infused composite aerostructures. Compos Sci Technol 2017;149:269–79. doi:10.1016/j.compscitech.2017.07.003.

[24] Mitchell CJ, Dangora LM, Sherwood JA. Investigation into a robust finite element model for composite materials. Finite Elem Anal Des 2016;115:1–8. doi:10.1016/j.finel.2016.02.003.

[25] Boisse P, Hamila N, Vidal-Salle E, Dumont F. Simulation of wrinkling during textile composite reinforcement forming. Influence of tensile, in-plane shear and bending stiffnesses. Compos Sci Technol 2011;71:683–92. doi:10.1016/j.compscitech.2011.01.011.

[26] Skordos AA, Monroy Aceves C, Sutcliffe MPF. A simplified rate dependent model of forming and wrinkling of pre-impregnated woven composites. Compos Part A Appl Sci Manuf 2007;38:1318–30. doi:10.1016/j.compositesa.2006.11.005.

[27] Harrison P, Gomes R, Curado-Correia N. Press forming a 0/90 cross-ply advanced thermoplastic composite using the double-dome benchmark geometry. Compos Part A Appl Sci Manuf 2013;54:56–69. doi:10.1016/j.compositesa.2013.06.014.

[28] Lin H, Long AC, Clifford M, Wang J, Harrison P. Predictive FE Modelling of Prepreg Forming to Determine Optimum Processing Conditions. AIP Conf Proc 2007;907:1092–7. doi:10.1063/1.2729660.

[29] Chen S, Harper LT, Endruweit A, Warrior NA. Composites : Part A Formability optimisation of fabric preforms by controlling material draw-in through in-plane constraints. Compos PART A 2015;76:10–9. doi:10.1016/j.compositesa.2015.05.006.

[30] Harrison P, Abdiwi F, Guo Z, Potluri P, Yu WR. Characterising the shear-tension coupling and wrinkling behaviour of woven engineering fabrics. Compos Part A Appl Sci Manuf 2012;43:903–14. doi:10.1016/j.compositesa.2012.01.024.

[31] Arnold SE, Sutcliffe MPF, Oram WLA. Experimental measurement of wrinkle formation during draping of non-crimp fabric. Compos Part A Appl Sci Manuf 2016;82:159–69. doi:10.1016/j.compositesa.2015.12.011.

[32] Mohan RP, Alshahrani H, Hojjati M. Investigation of intra-ply shear behavior of out-of-autoclave carbon/epoxy prepreg. J Compos Mater 2016;50:4251–4268. doi:10.1177/0021998316635238.

[33] Potter K. Bias extension measurements on cross-plied unidirectional prepreg. Compos - Part A Appl Sci Manuf 2002;33:63–73. doi:10.1016/S1359-835X(01)00057-4.

[34] Rashidi A, Milani AS. CHARACTERIZATION OF WRINKLING AND DE-WRINKLING BEHAVIOUR OF WOVEN FABRICS USING A MULTI-STEP BIAXIAL BIAS EXTENSION TEST. ECCM17 - 17th Eur. Conf. Compos. Mater., Munich, Germany: 2016, p. 26–30.

[35] Ferreira T, Rasband W. ImageJ User Guide. vol. 1.46r. 2012. doi:10.1038/nmeth.2019.